

The use of contrast-enhanced micro- CT for studying the forelimb musculature of the sparrowhawk (*Accipiter nisus*) (#14790)

1

First submission

Please read the **Important notes** below, the **Review guidance** on page 2 and our **Standout reviewing tips** on page 3. When ready [submit online](#). The manuscript starts on page 4.

Important notes

Editor and deadline

Virginia Abdala / 18 Dec 2016

Files

Please visit the overview page to [download and review](#) the files not included in this review PDF.

Declarations

No notable declarations are present



Please read in full before you begin

How to review






When ready [submit your review online](#). The review form is divided into 5 sections. Please consider these when composing your review:

- 1. BASIC REPORTING**
- 2. EXPERIMENTAL DESIGN**
- 3. VALIDITY OF THE FINDINGS**
4. General comments
5. Confidential notes to the editor





 You can also annotate this PDF and upload it as part of your review

To finish, enter your editorial recommendation (accept, revise or reject) and submit.

BASIC REPORTING

-  Clear, unambiguous, professional English language used throughout.
-  Intro & background to show context. Literature well referenced & relevant.
-  Structure conforms to [PeerJ standards](#), discipline norm, or improved for clarity.
-  Figures are relevant, high quality, well labelled & described.
-  Raw data supplied (see [PeerJ policy](#)).

EXPERIMENTAL DESIGN

-  Original primary research within [Scope of the journal](#).
-  Research question well defined, relevant & meaningful. It is stated how the research fills an identified knowledge gap.
-  Rigorous investigation performed to a high technical & ethical standard.
-  Methods described with sufficient detail & information to replicate.

VALIDITY OF THE FINDINGS

-  Impact and novelty not assessed. Negative/inconclusive results accepted. *Meaningful* replication encouraged where rationale & benefit to literature is clearly stated.
-  Data is robust, statistically sound, & controlled.
-  Conclusions are well stated, linked to original research question & limited to supporting results.
-  Speculation is welcome, but should be identified as such.

The above is the editorial criteria summary. To view in full visit <https://peerj.com/about/editorial-criteria/>

7 Standout reviewing tips

3



The best reviewers use these techniques

Tip

Example

Support criticisms with evidence from the text or from other sources

Smith et al (J of Methodology, 2005, V3, pp 123) have shown that the analysis you use in Lines 241-250 is not the most appropriate for this situation. Please explain why you used this method.

Give specific suggestions on how to improve the manuscript

Your introduction needs more detail. I suggest that you improve the description at lines 57- 86 to provide more justification for your study (specifically, you should expand upon the knowledge gap being filled).

Comment on language and grammar issues

The English language should be improved to ensure that your international audience can clearly understand your text. I suggest that you have a native English speaking colleague review your manuscript. Some examples where the language could be improved include lines 23, 77, 121, 128 - the current phrasing makes comprehension difficult.

Organize by importance of the issues, and number your points

1. Your most important issue
2. The next most important item
3. ...
4. The least important points

Give specific suggestions on how to improve the manuscript

Line 56: Note that experimental data on sprawling animals needs to be updated. Line 66: Please consider exchanging "modern" with "cursorial".

Please provide constructive criticism, and avoid personal opinions

I thank you for providing the raw data, however your supplemental files need more descriptive metadata identifiers to be useful to future readers. Although your results are compelling, the data analysis should be improved in the following ways: AA, BB, CC

Comment on strengths (as well as weaknesses) of the manuscript

I commend the authors for their extensive data set, compiled over many years of detailed fieldwork. In addition, the manuscript is clearly written in professional, unambiguous language. If there is a weakness, it is in the statistical analysis (as I have noted above) which should be improved upon before Acceptance.

The use of contrast-enhanced micro- CT for studying the forelimb musculature of the sparrowhawk (*Accipiter nisus*)

Fernanda Bribiesca-Contreras^{Corresp., 1}, William I. Sellers¹

¹ Faculty of Science and Engineering, University of Manchester, Manchester, United Kingdom

Corresponding Author: Fernanda Bribiesca-Contreras

Email address: fernanda.bribiesca@postgrad.manchester.ac.uk

Background. Gross dissection is a widespread method for studying animal anatomy, despite being highly destructive and time-consuming. X-ray computed tomography (CT) has been shown to be a non-destructive alternative for studying anatomical structures. However, in the past it has been limited to only being able to visualise mineralised tissues. In recent years, morphologists have started to use traditional X-ray contrast agents to allow the visualisation of soft tissue elements in the CT context. The aim of this project is to assess the ability of contrast-enhanced micro-CT (μ CT) to reconstruct a three-dimensional (3D) model of the musculoskeletal system of the bird wing and to quantify muscle geometry and any systematic changes due to shrinkage.

Methods. A 3% iodine-based buffered formalin solution with a two-week staining period was used to visualise the wing myology of the sparrowhawk (*Accipiter nisus*). μ CT scans of the wing were taken over the staining period until full penetration of the forelimb musculature by iodine was reached. A 3D model was reconstructed by manually segmenting out the individual elements of the avian wing with the help of 3D visualisation software.

Results. Different patterns of contrast are observed over the duration of the staining treatment with the best results occurring after 25 days of staining. The staining process made it possible to visualise and identify different elements of the soft tissue of the internal wing. Finally, a 3D reconstruction of the musculoskeletal system of the sparrowhawk wing is presented and numerical data of muscle geometry is compared to values obtained by dissection.

Discussion. Contrast-enhanced μ CT allows the visualisation and identification of the wing myology of birds, including the smaller muscles in the hand, and provides a non-destructive way for quantifying muscle architecture with an accuracy of 96.2%. By combining it with 3D visualisation techniques it is possible to study the individual muscles of the forelimb in their original position and 3D design, which can be the basis of further biomechanical analysis. Because the stain can be optionally washed out post analysis this technique provides a means of obtaining quantitative muscle data from museum specimens non-destructively.

1 **The use of contrast-enhanced micro- CT for studying the forelimb musculature of the**
 2 **sparrowhawk (*Accipiter nisus*)**

3 Fernanda Bribiesca-Contreras¹ and William I. Sellers¹

4 ¹ Faculty of Science and Engineering, University of Manchester, Manchester M13 9PT, UK.

5 Corresponding author:

6 Fernanda Bribiesca-Contreras¹

7 Email address: fernanda.bribiesca@postgrad.manchester.ac.uk

8 Abstract

9 **Background.** Gross dissection is a widespread method for studying animal anatomy, despite
10 being highly destructive and time-consuming. X-ray computed tomography (CT) has been shown
11 to be a non-destructive alternative for studying anatomical structures. However, in the past it has
12 been limited to only being able to visualise mineralised tissues. In recent years, morphologists
13 have started to use transdermal X-ray contrast agents to allow the visualisation of soft tissue
14 elements in the CT context. The aim of this project is to assess the ability of contrast-enhanced
15 micro-CT (μ CT) to reconstruct a three-dimensional (3D) model of the musculoskeletal system of
16 the bird wing and to quantify muscle geometry and any systematic changes due to shrinkage.

17 **Methods.** A 3% iodine-based buffered formalin solution with a two-week staining period was
18 used to visualise the wing myology of the sparrowhawk (*Accipiter nisus*). μ CT scans of the wing
19 were taken over the staining period until full penetration of the forelimb musculature by iodine
20 was reached. A 3D model was reconstructed by manually segmenting out the individual elements
21 of the avian wing with the help of 3D visualisation software.

22 **Results.** Different patterns of contrast enhancement were observed over the duration of the staining treatment
23 with the best results occurring after 25 days of staining. The staining process made it possible to
24 visualise and identify different elements of the soft tissue of the internal wing. Finally, a 3D
25 reconstruction of the musculoskeletal system of the sparrowhawk wing is presented and
26 numerical data of muscle geometry is compared to values obtained by dissection.

27 **Discussion.** Contrast-enhanced μ CT allows the visualisation and identification of the wing
28 myology of birds, including the smaller muscles in the hand, and provides a non-destructive way
29 for quantifying muscle architecture with an accuracy of 96.2%. By combining it with 3D
30 visualisation techniques it is possible to study the individual muscles of the forelimb in their
31 original position and 3D design, which can be the basis of further biomechanical analysis.
32 Because the stain can be optionally washed out post analysis this technique provides a means of
33 obtaining quantitative muscle data from museum specimens non-destructively.

34 **Keywords:** Birds, wing, 3D modelling, muscle architecture, staining.

35 Introduction

Gross dissection is undoubtedly the most commonly used technique for studying animal anatomy. This method makes possible a comprehensive analysis of the anatomical structure of any region of interest, enabling the visualisation of both hard and soft tissue elements and the measurement of morphological features. However, dissection is a time-consuming and highly destructive technique that does not allow the repetition of observations once the specimen has been dissected, which often makes it unsuitable for museum specimens.

X-ray computed tomography (CT) scanning is a non-destructive alternative that has become more widespread in medical and biological studies (Mizutani & Suzuki, 2012; Faulwetter et al., 2013; Lautenschlager, Bright & Rayfield, 2014). Nevertheless, X-ray CT scanning of untreated specimens has the disadvantage of being restricted to mineralized structures due to the low X-ray absorption capacity of soft tissue (Mizutani & Suzuki, 2012). To counteract this, morphologists have developed new approaches for imaging soft tissue by X-ray using staining treatments of anatomical structures with contrast-enhancing agents (Gignac et al., 2016). Contrast agents have been historically employed for studying soft tissue with light microscopy (e.g. gold and silver; Grizzle, 1996; Valverde, 1970), electron microscopy (e.g. osmium; Mizutani & Suzuki, 2012) and gross dissection (e.g. iodine; Bock & Shear, 1972). Moreover, they have been commonly employed in diagnostic medical X-rays since the early 1900s (Patton, 1994) and, recently, their use has extended to X-ray CT scanning technology. So far, a variety of agents (e.g. phosphotungstic acid (PTA), phosphomolybdic acid (PMA), osmium tetroxide and iodine-based solutions) have been tested in both vertebrates and invertebrates and have proved to be a suitable tool for soft tissue visualization of fishes (Metscher, 2009a; Descamps et al., 2014), amphibians (Metscher, 2009a; Kleinteich & Gorb, 2015), reptiles (Tsai & Holliday, 2011; Gröning et al., 2013), birds (Düring et al., 2013; Lautenschlager, Bright & Rayfield, 2014; Li et al., 2015; Hieronymus, 2016), mammals (Jeffery et al., 2011; Cox & Jeffery, 2011; Stephenson et al., 2012; Aslanidi et al., 2013; Baverstock, Jeffery & Cobb, 2013; Cox & Faulkes, 2014; Shearer et al., 2014), vertebrate embryos (Metscher, 2009b; Degenhardt et al., 2010; Tahara & Larsson, 2013; Descamps et al., 2014) and invertebrates (Metscher, 2009b; Faulwetter et al., 2013; Boyde et al., 2014).

In the last decade, iodine-based enhancing contrast μ CT has been preferred for imaging biological organisms and has proved successful for soft tissue visualisation on multiple anatomical studies (for a review, see Gignac et al., 2016). This technique involves treating the specimen with an iodine-based solution and consists of soaking the sample in an enclosed jar containing the staining agent for a specific amount of days. The most common iodine-based solution is Lugol's iodine, or iodine-potassium iodide (I_2KI), that is composed of two parts of KI for each part of I_2 dissolved in an aqueous solution (Gignac et al., 2016). It gained popularity after being tested on embryos, vertebrates and invertebrates in a comparative study of the effectiveness of multiple staining agents for enhancing contrast of soft tissues (Metscher, 2009b). In the work of Metscher (2009a), Lugol's solution proved to be an effective agent for soft tissue visualisation in both vertebrates and invertebrates. Other staining agents have achieved similar results, or even slightly better (e.g. PTA; Metscher, 2009a; Pauwels et al., 2013; osmium tetroxide; Metscher, 2009a,b; Mizutani & Suzuki, 2012), however, iodine has the advantages of being easily available, relatively inexpensive, easy to manipulate and shows strong affinity for major types of soft tissue (Metscher, 2009b; Gignac et al., 2016). In particular, iodine-based contrast-enhanced μ CT has been commonly employed for investigating skeletal muscles as it has been observed that iodine seems to have a strong affinity for muscle fibres and muscle fascia (Cox & Jeffery, 2011; Tsai & Holliday, 2011; Aslanidi et al., 2013; Baverstock, Jeffery & Cobb, 2013), which makes this technique a suitable approach for three-dimensional reconstruction of musculature that can be useful for further biomechanical analysis (Baverstock, Jeffery & Cobb, 2013; Gröning et al., 2013; Kleinteich & Gorb, 2015). Likewise, it makes possible the measurement of muscle geometry parameters such as muscle volumes (de Crespigny et al., 2008; Baverstock, Jeffery & Cobb, 2013) and fascicle length (Jeffery et al., 2011) which can otherwise be difficult to estimate accurately.

For iodine-based CT scanning, different methodologies have been followed that depend on the sample type, specimen treatment prior to staining, staining duration and contrast agent properties. Some authors have chosen different solutions for dissolving I_2KI such as ethanol (I_2E ; e.g. Stephenson et al., 2012; Silva et al., 2015), methanol (I_2M ; Metscher, 2009b) or water (I_2KI or Lugol's solution; for review, see Gignac et al., 2016). However, it has been demonstrated that ethanol increases tissue shrinkage, thus is not recommended when morphological measurements are fundamental (Vickerton, Jarvis & Jeffery, 2013). Lower or higher concentration of iodine has

indiscriminately been preferred, however, it seems that the size of the specimen to be imaged is relevant when deciding the solution concentration and duration treatment. As the specimen gets smaller, the distance the iodine has to diffuse in order to reach deeper structures gets shorter; therefore, a lower concentration of I₂KI is required and a shorter staining duration can be used (Gignac et al., 2016). Simultaneously, the opposite occurs in larger specimens, which demand higher I₂KI concentration and longer staining durations. Unfortunately, decomposition of tissue can occur after longer staining periods in larger specimens so it is important to choose the correct staining solution and duration for a particular specimen. An example of this is shown by Li et al. (2015) who employed a protocol for imaging larger specimens over a longer duration using a modified iodine-based buffered formalin solution at a low concentration. This avoided damage of the tissues despite the longer staining period and the lower concentration helped to minimise shrinkage (Degenhardt et al., 2010; Vickerton, Jarvis & Jeffery, 2013).

The aim of the present work is to test the utility of iodine-based contrast-enhanced μ CT for studying the myology of the avian forelimb since whilst they are relatively large animals, the diffusion distance is relatively large and the appropriate protocol for wing soft tissue is currently unknown. The process was undertaken using a sparrowhawk (*Accipiter nisus*) wing as a model but we expect that the findings will generalise to wing studies in other birds. To do this, a low concentration iodine-based buffered formalin solution was preferred in order to avoid damage of the tissues, as the duration of the staining was uncertain, and CT scans were taken at stepped time increments. In addition, numerical data of muscle geometry was obtained for comparison with quantitative dissections to assess the impact of shrinkage on muscle volumes.

Methods

Specimen treatment. The left wing of an adult female sparrowhawk (*Accipiter nisus*) was used for this study. The specimen was donated from the World Museum of Liverpool and kept frozen at -20°C before use and then left to thaw overnight before dissection. The wing was dislocated free from the shoulder by cutting the origin tendons and fleshy attachments of the shoulder and pectoral muscles. After being plucked and skinned, it was fixed in 10% Neutral Buffered Formalin (NBF) and stored in a fridge at 3°C for two weeks. For staining, it was transferred to a ~3% (w/v) iodine-based buffered formalin solution in an enclosed jar. The staining solution was

prepared using the method described by Li et al. (2015) for larger specimens (8 g iodine, 16 g potassium iodide into 800 ml 10% NBF). The choice of a lower concentration of contrast agent was made to avoid shrinkage of the tissues as it has been previously observed that soft tissue shrinkage increases with higher concentrations of iodine (Tahara & Larsson, 2013; Vickerton, Jarvis & Jeffery, 2013; Gignac & Kley, 2014).

Imaging. For imaging, the wing was removed from the fixing and staining solution and scanned with a Nikon XTEK XTH 225 kV μ CT system at the Henry Moseley X-ray Imaging Facility, University of Manchester. Before each scan, the wing was removed from the solution and rinsed with water to remove excess of stain and to prevent surface saturation. A first scan of the unstained wing (70 kV, 200 μ A) was taken on day 1 to act as a control image, followed by scans of the stained wing on days 4, 11, 16, 19 and 26 (80 kV, 100 μ A, 0.25 mm aluminium filter) to allow comparison of the contrast achieved for the different staining durations. Each time, three separate scans were taken of the regions of interest (brachial arm, antebrachial arm and hand) at the same position to facilitate further merging of the whole wing in a single file, which was done by aligning the volume rendering of the three sections and then applying the “Merge” module in Avizo (version Lite 9.0, Visualisation Centre Group). A total of 5013 projections were obtained over 360°, resulting in an acquisition time of 1 hour 24 minutes (4 hours 12 minutes in total for the whole wing) at a resolution of 25 μ m/voxel for each region of interest.

Reconstruction of 3D model. Reconstruction of the wing from the CT images was carried out with the Nikon Metrology NV CT-Pro reconstruction software (version V4.0.5360.28810, September 2014) and imported into Avizo (version Lite 9.0, Visualisation Centre Group) for further visualisation and segmentation of individual anatomical elements. Each muscle and bone was manually segmented out using both the “magic wand” and “painting brush” tools, and interpolating between 5-10 slices. This was preferred over the “threshold” option due to the similarity in grey-scale intensity between bones and muscles as a consequence of the radiodensity reached during the staining treatment, although they could be clearly recognized independently from each other by a human operator, as reported in similar studies (Cox & Jeffery, 2011; Baverstock, Jeffery & Cobb, 2013; Lautenschlager, Bright & Rayfield, 2014; Cox & Faulkes, 2014). Isosurfaces of the volumes of the elements segmented out were generated to build a three-

dimensional model of the wing in order to visualise the hard and soft tissue forming the bird forelimb. Furthermore, isosurfacing allows the calculation of the volume of each muscle by means of the Avizo “measure and analyse module”. Muscles volumes were compared to the muscle volumes calculated from the muscle masses of the wing and a standard value for muscle density both after the stain was washed out, and also by comparison with the fresh wing (right wing of the same individual) measured during dissection. A standard value of muscle density for vertebrate skeletal muscle was used ($1.06 \text{ g}\cdot\text{cm}^{-3}$; Mendez and Keys, 1960; Brown et al., 2003).

Results

Visualisation of both soft and hard tissue of the bird wing was possible over the duration of the staining treatment with an iodine-based buffered formalin solution. Different patterns of contrast are observed along the 25 days of the staining procedure, as are shown in Fig. 1. The control image (Fig.1; A) only showed detail of the bones while the distinct elements of the soft tissue are unrecognized. An improvement of contrast is evident as the duration of staining increases (Fig 1; B-F). Moreover, it can be observed that it takes longer for the iodine solution to reach into deeper muscles such as the arm musculature (Fig. 1; first row), where a clear visualisation of all the muscles is not achieved until the last day of the treatment. In comparison, the smaller muscles of the distal wing (Fig 1; third row) were rapidly stained after only three days of treatment.

Furthermore, the contrast-enhanced μCT images of the bird wing demonstrate different attenuation among the tissues. Fig. 2 shows more detailed images of the anatomical sections of the wing where it is possible to recognise elements of the connective tissue separating the muscles and remains of the skin in the hand. It seems to have a low affinity for ligaments and tendons as it can be observed in, for example, the muscle *flexor carpi ulnaris* where the dark area corresponds to the internal tendon of this muscle (black arrow in Fig. 2B). Since tendon morphology can be an important component of biomechanical analysis this is potentially an important consideration (Sellers et al., 2010).

A 3D model of the musculoskeletal system of the sparrowhawk wing is presented in Figure 3 showing the 30 muscles comprising the avian forelimb. This clearly illustrates the value of this

technique for reconstructing the 3D shape of the individual muscles and their anatomical relations which can be essential for biomechanical models (Sellers et al., 2013). However it also illustrates that little stain is taken up by other soft tissues and in particular reinforces the observation of an almost complete lack of staining in the tendons (e.g. distal attachment of *biceps brachii*).

Figure 4 shows the regression analysis for the wing muscles volumes of the fresh wing and 3D model resulted in a slope of 0.6366 ($R^2 = 0.962$), indicating a linear relationship between the volumes muscles obtained from the model isosurfaces and the data calculated from the dissection of the fresh wing ($p < 0.001$). This result validates the use of 3D imaging techniques for obtaining quantitative data of muscle architecture although the slope shows that there is appreciable shrinkage (3%), which needs to be taken into consideration to obtain useful quantitative data.

Discussion

Contrast-enhanced μ CT using an iodine-based buffered formalin solution produces highly detailed visualisation and identification of the different muscles forming the avian wing. During the staining treatment of the sparrowhawk wing, it is evident that it takes longer for the iodine to reach deeper and larger muscles (Fig. 1). In the case of the hand that comprises the smaller muscles in the wing, full contrast of the muscles was reached during the first three days of staining and can be easily identified in independent units after 10 days (Fig. 1B). In contrast, it took much longer for the brachial musculature that includes the larger muscles of the wing. After two weeks, individual muscles can be identified although the dark area near the skeleton indicates that the iodine has not yet reached the deeper fibres of the larger muscles, such as the *scapulotriceps* (ST) (Fig. 1D). These different patterns in the improvement of contrast over the duration of the treatment, illustrates a relationship between enhancing contrast with the specimen size and duration of the staining and are thus important to consider when designing a staining protocol (Tahara & Larsson, 2013; Li et al., 2015; Gignac et al., 2016).

The technique has proven to be effective for revealing the different soft elements comprising the musculoskeletal system of the sparrowhawk wing. Individual muscles are clearly distinguished by means of the contrast agent solution on staining the fascia separating them (Fig. 2) and even

muscle fibres are distinguished in the tiny muscles of the hand (Fig. 1, 2). It is believed that iodine adheres to different constituents of tissues, such as glycogen and lipids (Metsc 2009b; Mizutani & Suzuki, 2012), and that it has a strong affinity for muscle fascia and muscle fibres (Jeffery et al., 2011; Tsai & Holliday, 2011; Baverstock, Jeffery & Cobb, 2013) and internal structures of ligaments and tendons (Shearer et al., 2014). However, our results do not show the insertion and origin tendons of the wing muscles, indicating a poor affinity of the iodine with these structures so we would suggest that this protocol is not suitable if tendon visualisation is the primary goal of the study. It is possible to visualise the internal tendons of some muscles as dark areas of low attenuation inside the muscles such as in the muscle *flexor carpi ulnaris* (FCU; Fig. 2B). Using an alternative contrast agent, such as PTA and PMA that are known to bind to collagen fibres (Mizutani & Suzuki, 2012; Pauwels et al., 2013; Descamps et al., 2014; Shearer et al., 2014), may help us to visualise tendinous structures of the wing muscles of the sparrowhawk. This was recently achieved by Hieronymus (2016), who developed a comprehensive 3D model of the internal anatomy of the rock pigeon by combining μ CT scanning and histological sectioning to study the anatomical structures that shape the wing during flight. Increasing the duration of the staining treatment might improve the visibility of the wing tendons as well, since it was possible to observe the surface and internal structure of the anterior cruciate ligament and patellar tendon in porcine specimens after 70 days of staining with I_2KI (Shearer et al., 2014) but this is considerably longer than the duration of the current experiment and may also be related to the diffusion distance in these larger specimens (Gignac et al., 2016). With prolonged staining periods there is also a risk of the muscles being over-stained which would reduce the visualisation of other important soft-tissues (Gignac & Kley, 2014; Gignac et al., 2016).

Our results show that contrast-enhanced μ CT using an iodine-based buffered formalin solution is a suitable technique for visualising and identifying the different muscles forming the avian wing. By combining it with 3D visualisation techniques, it is possible to study the wing muscles design in their original position, which is very difficult to assess accurately during gross dissections where anatomical structures are commonly damaged or precise 3D relationships are difficult to discern (Lautenschlager, Bright & Rayfield, 2014) and deeper structures are difficult to reach (Cox & Jeffery, 2011; Cox & Faulkes, 2014). The 3D model provided in this work can be used as an anatomical and dissection guide of the wing musculature, in particular of the smaller muscles

of the hands that attach directly to the bones for which only a few illustrated descriptions are available (Vazquez, 1995; Zhang & Yang, 2013; Yang, Wang & Zhang, 2015; Hieronymus, 2016); however, care must be taken due to the lack of tendons in this reconstruction and this is an area where more work is clearly required.

Furthermore, this 3D model can be employed for further investigation of functional morphology and biomechanics of the forelimb musculature, as this technique proved to be a non-destructive alternative for obtaining quantitative data of muscle architecture as required for advanced biomechanical techniques such as multibody-dynamics analysis (Jeffery et al., 2011; Gröning et al., 2013). Nevertheless, when using this technique for obtaining accurate numerical data of muscle geometry it is still essential to normalise the data against dissection data because significant shrinkage is present even when using a lower concentration of iodine (Li et al., 2015; Gignac et al., 2016), as we noticed after comparing with the fresh wing of the same individual during dissection where a shrinkage of ~33% occurred after 25 days of staining (Fig. 4). Similar results have been reported for skeletal muscle in mice with 2% I₂KI (Vickerton, Jarvis & Jeffery, 2013) and New Zealand rabbits with 3% I₂KI (Buytaert et al., 2014) that presented ~20% and 34-48% of shrinkage, respectively, in muscle volume after the staining treatment.

Conclusions

Contrast-enhanced μ CT has been demonstrated to be a suitable non-destructive alternative of gross dissection for studying the wing musculature of birds. By using a low concentration of an iodine-based buffered formalin solution for a two-week staining period, it was possible to visualise and identify all the individual muscles of the bird wing; however, staining of tendons was not achieved. Therefore, it is recommended to test the use of alternative contrast agents (*e. g.* PTA or PMA) for a full assessment of the anatomical elements forming the musculoskeletal system of the avian wing. Finally, we presented a 3D model of the internal anatomy of the sparrowhawk wing by combining contrast-enhanced μ CT with 3D visualisation techniques where it is possible to see the muscles arrangement in their original anatomical position. In addition, it is possible to obtain quantitative data of muscle architecture from this model that, after normalising

with numerical dissection data, can be useful for further biomechanical analysis and functional morphology predictions of the role of individual muscles during flapping flight.

Acknowledgments

We are grateful to Julia Behnsen and Charlotte Brassey for their help and suggestions during the CT scanning and 3D modelling and to Tony Parker for the donation of the specimen used in this project. We also thank Ben Parslew for discussion and helpful comments that improved this manuscript.

References

- Aslanidi OV., Nikolaidou T., Zhao J., Smaill BH., Gilbert SH., Holden AV., Lowe T., Withers PJ., Stephenson RS., Jarvis JC., Hancox JC., Boyett MR., Zhang H. 2013. Application of micro-computed tomography with iodine staining to cardiac imaging, segmentation, and computational model development. *IEEE transactions on medical imaging* 32:8–17. DOI: 10.1109/TMI.2012.2209183.
- Baverstock H., Jeffery NS., Cobb SN. 2013. The morphology of the mouse masticatory musculature. *Journal of Anatomy* 223:46–60. DOI: 10.1111/joa.12059.
- Bock WJ., Shear CR. 1972. A staining method for gross dissection of vertebrate muscles. *Anatomischer Anzeiger* 130:222–227.
- Boyde A., Mccorkell FA., Taylor GK., Bompfrey RJ., Doube M. 2014. Iodine vapor staining for atomic number contrast in backscattered electron and X-ray imaging. *Microscopy Research and Technique* 77:1044–1051. DOI: 10.1002/jemt.22435.

- 285 Brown NA., Pandy MG., Kawcak CE., McIlwraith CW. 2003. Force- and moment-generating
286 capacities of muscles in the distal forelimb of the horse. *Journal of Anatomy* 203:101–
287 113. DOI: 10.1046/j.1469-7580.2003.00206.x.
- 288 Buytaert J., Goyens J., Greef DD., Aerts P., Dirckx J. 2014. Volume Shrinkage of Bone, Brain
289 and Muscle Tissue in Sample Preparation for Micro-CT and Light Sheet Fluorescence
290 Microscopy (LSFM). *Microscopy and Microanalysis* 20:1208–1217. DOI:
291 10.1017/S1431927614001329.
- 292 Cox PG., Faulkes CG. 2014. Digital dissection of the masticatory muscles of the naked mole-rat,
293 *Heterocephalus glaber* (Mammalia, Rodentia). *PeerJ* 2. DOI: 10.7717/peerj.448.
- 294 Cox PG., Jeffery N. 2011. Reviewing the morphology of the jaw-closing musculature in
295 squirrels, rats, and guinea pigs with contrast-enhanced microCT. *Anatomical Record*
296 (*Hoboken, N.J.: 2007*) 294:915–928. DOI: 10.1002/ar.21381.
- 297 de Crespigny A., Bou-Reslan H., Nishimura MC., Phillips H., Carano RAD., D’Arceuil HE.
298 2008. 3D micro-CT imaging of the postmortem brain. *Journal of Neuroscience Methods*
299 171:207–213. DOI: 10.1016/j.jneumeth.2008.03.006.
- 300 Degenhardt K., Wright AC., Horng D., Padmanabhan A., Epstein JA. 2010. Rapid 3D
301 phenotyping of cardiovascular development in mouse embryos by micro-CT with iodine
302 staining. *Circ Cardiovasc Imag* 3. DOI: 10.1161/CIRCIMAGING.109.918482.
- 303 Descamps E., Sochacka A., De Kegel B., Van Loo D., Van Hoorebeke L., Adriaens D. 2014. Soft
304 tissue discrimination with contrast agents using micro-CT scanning. *Belg J Zool* 144:20–
305 40.
- 306 Düring DN., Ziegler A., Thompson CK., Ziegler A., Faber C., Müller J., Scharff C., Elemans CP.
307 2013. The songbird syrinx morphome: a three-dimensional, high-resolution, interactive

308 morphological map of the zebra finch vocal organ. *BMC Biology* 11:1. DOI:
 309 10.1186/1741-7007-11-1.

310 Faulwetter S., Vasileiadou A., Kouratoras M., Dailianis T., Arvanitidis C. 2013. Micro-computed
 311 tomography: Introducing new dimensions to taxonomy. *ZooKeys* 263. DOI:
 312 10.3897/zookeys.263.4261.

313 Gignac PM., Kley NJ. 2014. Iodine-enhanced micro-CT imaging: Methodological refinements
 314 for the study of the soft-tissue anatomy of post-embryonic vertebrates. *Journal of*
 315 *Experimental Zoology Part B: Molecular and Developmental Evolution* 322:166–176.
 316 DOI: 10.1002/jez.b.22561.

317 Gignac PM., Kley NJ., Clarke JA., Colbert MW., Morhardt AC., Cerio D., Cost IN., Cox PG.,
 318 Daza JD., Early CM., Echols MS., Henkelman RM., Herdina AN., Holliday CM., Li Z.,
 319 Mahlow K., Merchant S., Müller J., Orsbon CP., Paluh DJ., Thies ML., Tsai HP., Witmer
 320 LM. 2016. Diffusible iodine-based contrast-enhanced computed tomography (diceCT): an
 321 emerging tool for rapid, high-resolution, 3-D imaging of metazoan soft tissues. *Journal of*
 322 *Anatomy*:n/a–n/a. DOI: 10.1111/joa.12449.

323 Grizzle WE. 1996. Theory and Practice of Silver Staining in Histopathology. *Journal of*
 324 *Histotechnology* 19:183–195. DOI: 10.1179/his.1996.19.3.183.

325 Gröning F., Jones MEH., Curtis N., Herrel A., O’Higgins P., Evans SE., Fagan MJ. 2013. The
 326 importance of accurate muscle modelling for biomechanical analyses: a case study with a
 327 lizard skull. *Journal of The Royal Society Interface* 10:20130216. DOI:
 328 10.1098/rsif.2013.0216.

- 329 Hieronymus TL. 2016. Flight feather attachment in rock pigeons (*Columba livia*): covert feathers
330 and smooth muscle coordinate a morphing wing. *Journal of Anatomy* 229:631–656. DOI:
331 10.1111/joa.12511.
- 332 Jeffery NS., Stephenson RS., Gallagher JA., Jarvis JC., Cox PG. 2011. Micro-computed
333 tomography with iodine staining resolves the arrangement of muscle fibres. *Journal of*
334 *Biomechanics* 44:189–192. DOI: 10.1016/j.jbiomech.2010.08.027.
- 335 Kleinteich T., Gorb SN. 2015. Frog tongue acts as muscle-powered adhesive tape. *Royal Society*
336 *Open Science* 2. DOI: 10.1098/rsos.150333.
- 337 Lautenschlager S., Bright JA., Rayfield EJ. 2014. Digital dissection – using contrast-enhanced
338 computed tomography scanning to elucidate hard- and soft-tissue anatomy in the
339 Common Buzzard *Buteo buteo*. *Journal of Anatomy* 224:412–431. DOI:
340 10.1111/joa.12153.
- 341 Li Z., Clarke JA., Ketcham RA., Colbert MW., Yan F. 2015. An investigation of the efficacy and
342 mechanism of contrast-enhanced X-ray Computed Tomography utilizing iodine for large
343 specimens through experimental and simulation approaches. *BMC Physiology* 15. DOI:
344 10.1186/s12899-015-0019-3.
- 345 Mendez J., Keys A. 1960. Density and composition of mammalian muscle. *Metabolism-Clinical*
346 *and Experimental* 9:184–188.
- 347 Metscher BD. 2009a. MicroCT for developmental biology: A versatile tool for high-contrast 3D
348 imaging at histological resolutions. *Dev Dyn* 238. DOI: 10.1002/dvdy.21857.
- 349 Metscher BD. 2009b. MicroCT for comparative morphology: simple staining methods allow
350 high-contrast 3D imaging of diverse non-mineralized animal tissues. *BMC Physiol* 9.
351 DOI: 10.1186/1472-6793-9-11.

- 352 Mizutani R., Suzuki Y. 2012. X-ray microtomography in biology. *Micron* 43:104–115. DOI:
353 10.1016/j.micron.2011.10.002.
- 354 Patton DD. 1994. Insight on the radiologic centennial: a historical perspective. Part 4. Of
355 gastrointestinal radiology, bread and butter; or, the flowering of barium sulfate.
356 *Investigative Radiology* 29:472–479.
- 357 Pauwels E., Van Loo D., Cornillie P., Brabant L., Van Hoorebeke L. 2013. An exploratory study
358 of contrast agents for soft tissue visualization by means of high resolution X-ray
359 computed tomography imaging. *Journal of Microscopy* 250:21–31. DOI:
360 10.1111/jmi.12013.
- 361 Sellers WI., Margetts L., Coria RA., Manning PL. 2013. March of the Titans: The Locomotor
362 Capabilities of Sauropod Dinosaurs. *PLOS ONE* 8:e78733. DOI:
363 10.1371/journal.pone.0078733.
- 364 Sellers WI., Pataky TC., Caravaggi P., Crompton RH. 2010. Evolutionary Robotic Approaches in
365 Primate Gait Analysis. *International Journal of Primatology* 31:321–338. DOI:
366 10.1007/s10764-010-9396-4.
- 367 Shearer T., Rawson S., Castro SJ., Balint R., Bradley RS., Lowe T., Vila-Comamala J., Lee PD.,
368 Cartmell SH. 2014. X-ray computed tomography of the anterior cruciate ligament and
369 patellar tendon. *Muscles, Ligaments and Tendons Journal* 4:238–244.
- 370 Silva JM de S e., Zanette I., Noël PB., Cardoso MB., Kimm MA., Pfeiffer F. 2015. Three-
371 dimensional non-destructive soft-tissue visualization with X-ray staining micro-
372 tomography. *Scientific Reports* 5. DOI: 10.1038/srep14088.
- 373 Stephenson RS., Boyett MR., Hart G., Nikolaidou T., Cai X., Corno AF., Alphonso N., Jeffery
374 N., Jarvis JC. 2012. Contrast Enhanced Micro-Computed Tomography Resolves the 3-

375 Dimensional Morphology of the Cardiac Conduction System in Mammalian Hearts. *PLoS*
376 *ONE* 7. DOI: 10.1371/journal.pone.0035299.

377 Tahara R., Larsson HC. 2013. Quantitative analysis of microscopic X-ray computed tomography
378 imaging: Japanese quail embryonic soft tissues with iodine staining. *J Anat* 223. DOI:
379 10.1111/joa.12081.

380 Tsai HP., Holliday CM. 2011. Ontogeny of the Alligator Cartilago Transiliens and Its
381 Significance for Sauropsid Jaw Muscle Evolution. *PLoS ONE* 6. DOI:
382 10.1371/journal.pone.0024935.

383 Valverde F. 1970. The Golgi Method. A Tool for Comparative Structural Analyses. In: Nauta
384 WJH, Ebbesson SOE eds. *Contemporary Research Methods in Neuroanatomy*. Berlin,
385 Heidelberg: Springer Berlin Heidelberg, 12–31.

386 Vazquez RJ. 1995. Functional anatomy of the pigeon hand (*Columba livia*): A muscle stimulation
387 study. *Journal of Morphology* 226:33–45. DOI: 10.1002/jmor.1052260104.

388 Vickerton P., Jarvis J., Jeffery N. 2013. Concentration-dependent specimen shrinkage in iodine-
389 enhanced microCT. *J Anat* 223. DOI: 10.1111/joa.12068.

390 Yang Y., Wang H., Zhang Z. 2015. Muscle architecture of the forelimb of the Golden Pheasant
391 (*Chrysolophus pictus*) (Aves: Phasianidae) and its implications for functional capacity in
392 flight. *Avian Research* 6:1–8. DOI: 10.1186/s40657-015-0013-2.

393 Zhang Z., Yang Y. 2013. Forelimb Myology of the Golden Pheasant (*Chrysolophus pictus*).
394 *International Journal of Morphology* 31:1482–1490.

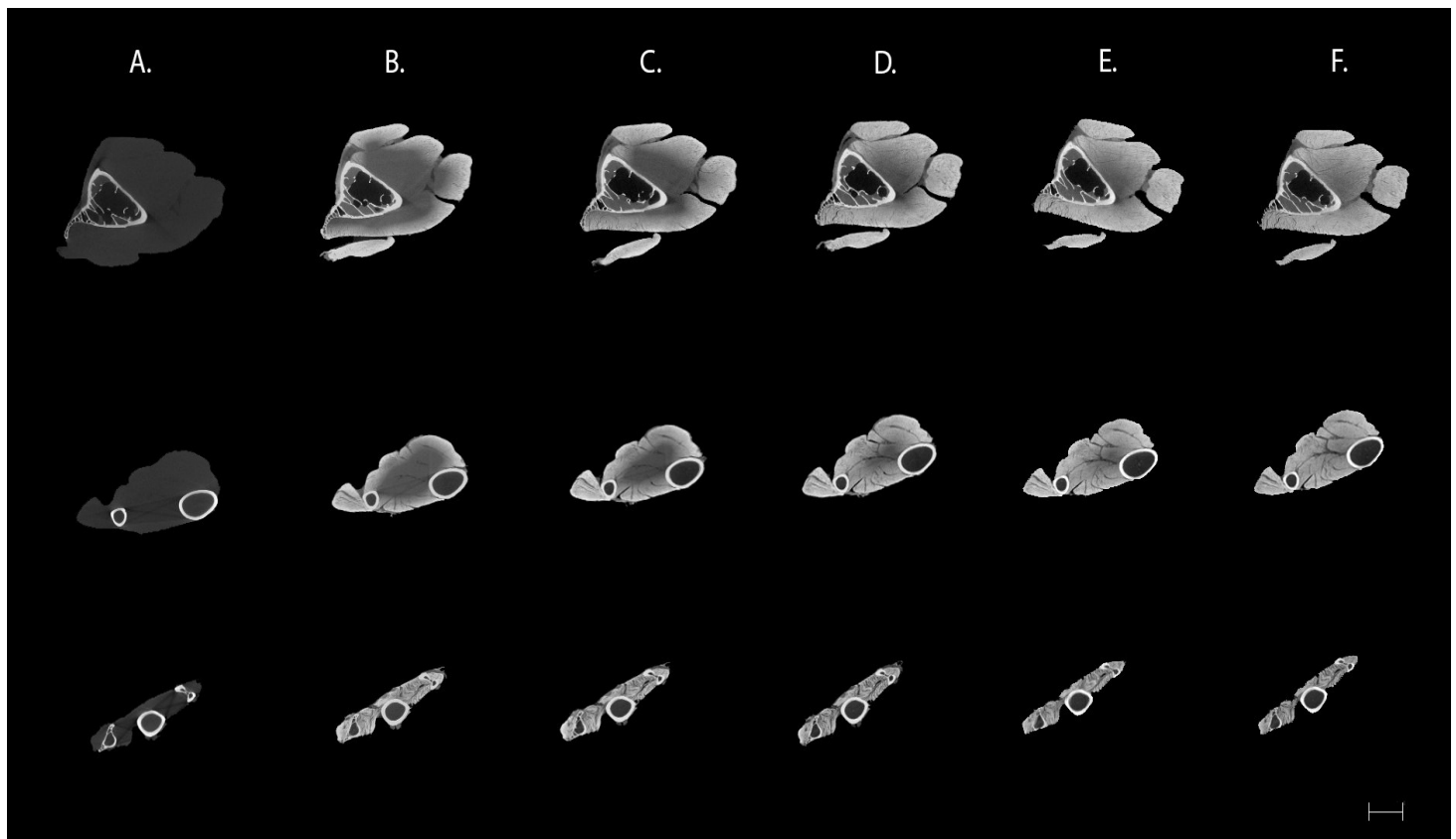


Figure 1. Transverse μ CT images of a sparrowhawk (*A. nisus*) wing. First row corresponds to the brachial arm, the second the antebrachial area and the third the avian hand. A. Control. B-F. ~3% (w/v) iodine-based buffered formalin solution for 3 (B), 10 (C), 15 (D), 18 (E) and 25 (F) days. Scale bar equal to 5 mm.

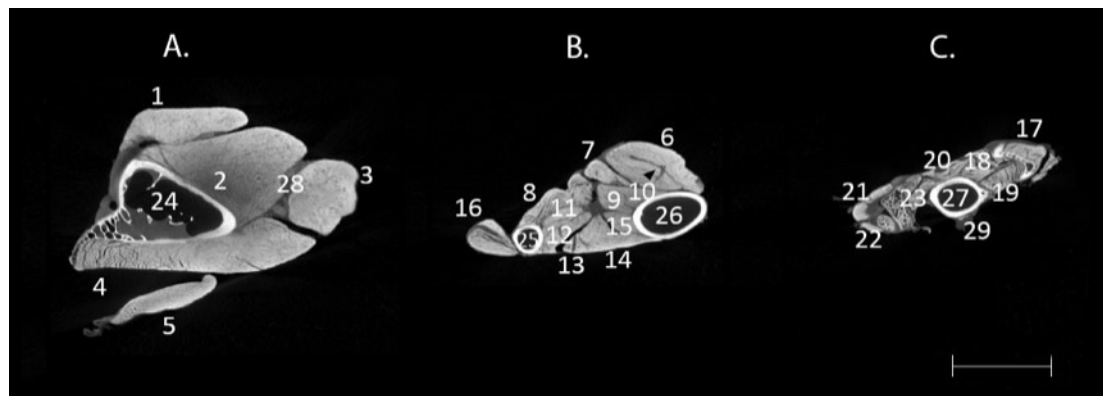


Figure 2. Transverse μ CT images of *A. nissus* in a ~3% (w/v) iodine-based buffered formalin solution for 25 days showing hard and soft tissue elements of the brachial arm (A), antebrachial (B) and hand (C). Black arrow shows at an area of low attenuation corresponding to the internal tendon of FCU (6). 1, BB; 2, ST; 3, HT; 4, DMA; 5, TPLA; 6, FCU; 7, FDS; 8, PP; 9, FDP; 10, UMV; 11, ELDM; 12, ELA; 13, EDC; 14, ECU; 15, ECTU; 16, EMR; 17, UMD; 18, ISD; 19, ISV; 20, ABDM; 21, ABA; 22, EBA; 23, ADA; 24, HUM; 25, R; 26, U; 27, CMC; 28, fascia; 29, skin. Abbreviations as indicated in Fig. Scale bar equal to 5 mm.

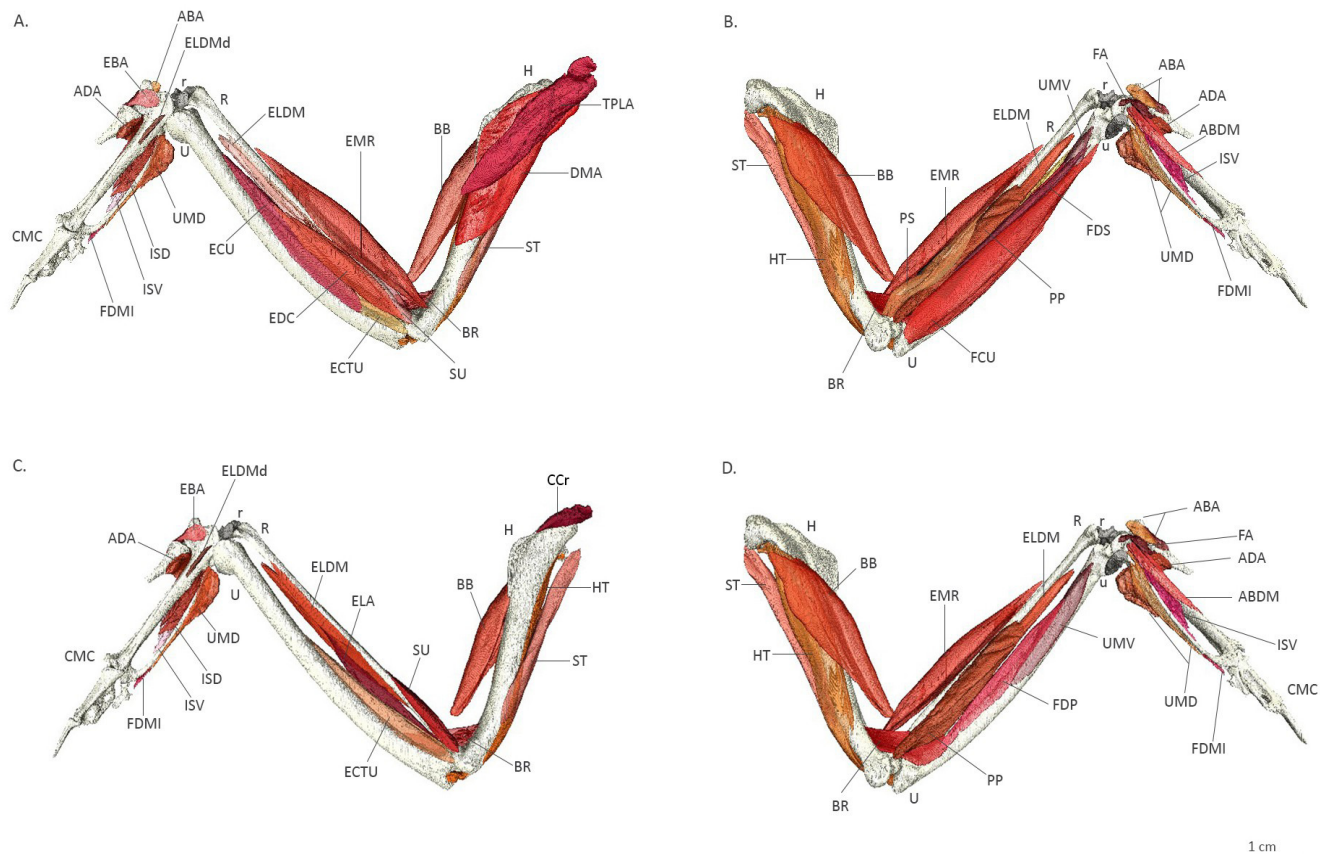


Figure 3. Wing muscles of a sparrowhawk. Dorsal view of superficial (A) and deep (C) muscles and ventral view of superficial (B) and deep (D) muscles. Abbreviations: TPLA, *tensor propatagialis pars longa*; DMA, *deltoides major*; CCr, *coracobrachialis cranialis*; BB, *biceps brachii*; ST, *scapulotriceps*; HT, *humerotriceps*; BR, *brachialis*; PP, *pronator profundus*; PS, *pronator superficialis*; ECTU, *ectepicondylus ulnaris*; FCU, *flexor carpi ulnaris*; FDS, *flexor digitorum superficialis*; FDP, *flexor digitorum profundus*; UMV, *ulnometacarpalis ventralis*; EMR, *extensor metacarpi radialis*; SU, *supinator*; EDC, *extensor digitorum communis*; ECU, *extensor carpi ulnaris*; ELA, *extensor longus alulae*; ELDM, *extensor longus digiti majoris*; ELDMd, *extensor longus digiti majoris pars distalis*; UMD, *ulnometacarpalis dorsalis*; ISD, *interosseus dorsalis*; ISV, *interosseus ventralis*; ABA, *abductor alulae*; ADA, *adductor alulae*; EBA, *extensor brevis alulae*; FA, *flexor alulae*; ABDM, *abductor digiti majoris*; FDMI, *flexor digiti minoris*; HUM, *humerus*; R, *radio*; U, *ulna*; r, *radiale*; u, *ulnare*; CMC, *carpometacarpus*.

